JCI insight

RESEARCH ARTICLE

CX3CR1^{-}CD8^{+} T cells are critical in antitumor efficacy but functionally suppressed in the tumor microenvironment

Takayoshi Yamauchi,[1,2] Toshifumi Hoki,[1,3] Takaaki Oba,[1] Hidehito Saito,[4,5] Kristopher Attwood,[6] Michael S. Sabel,[4] Alfred E. Chang,[4] Kunle Odunsi,[1,7,8] and Fumito Ito[1,4,9,10]

[1]Center for Immunotherapy, Roswell Park Comprehensive Cancer Center, Buffalo, New York, USA. [2]Department of Cell Signaling and Metabolic Medicine, Faculty of Life Sciences, Kumamoto University, Kumamoto, Japan. [3]Oncology Science Unit, MSD Japan, Tokyo, Japan. [4]Department of Surgery, University of Michigan, Ann Arbor, Michigan, USA. [5]Department of Biochemistry, Kanazawa Medical University School of Medicine, Kahoku, Japan. [6]Department of Biostatistics and Bioinformatics, [7]Department of Gynecologic Oncology, [8]Department of Immunology, and [9]Department of Surgical Oncology, Roswell Park Comprehensive Cancer Center, Buffalo, New York, USA. [10]Department of Surgery, Jacobs School of Medicine and Biomedical Sciences, State University of New York at Buffalo, Buffalo, New York, USA.

Although blockade of the programmed cell death 1/programmed cell death ligand 1 (PD-1/PD-L1) immune checkpoint has revolutionized cancer treatment, how it works on tumor-infiltrating CD8^{+} T cells recognizing the same antigen at various differentiation stages remains elusive. Here, we found that the chemokine receptor CX3CR1 identified 3 distinct differentiation states of intratumor CD8^{+} T cell subsets. Adoptively transferred antigen-specific CX3CR1^{-}CD8^{+} T cells generated phenotypically and functionally distinct CX3CR1^{int} and CX3CR1^{hi} subsets in the periphery. Notably, expression of coinhibitory receptors and T cell factor 1 (Tcf1) inversely correlated with the degree of T cell differentiation defined by CX3CR1. Despite lower expression of coinhibitory receptors and potent cytolytic activity, in vivo depletion of the CX3CR1^{hi} subset did not alter the antitumor efficacy of adoptively transferred CD8^{+} T cells. Furthermore, differentiated CX3CR1^{int} and CX3CR1^{hi} subsets were impaired in their ability to undergo proliferation upon restimulation and had no impact on established tumors upon second adoptive transfer compared with the CX3CR1^{-} subset that remained effective. Accordingly, anti–PD-L1 therapy preferentially rescued proliferation and cytokine production of the CX3CR1^{-} subset and enhanced antitumor efficacy of adoptively transferred CD8^{+} T cells. These findings provide a better understanding of the phenotypic and functional heterogeneity of tumor-infiltrating CD8^{+} T cells and can be exploited to develop more effective immunotherapy.

Introduction

CD8^{+} T cells are a critical component of adaptive immunity against intracellular pathogens and cancerous cells (1). Upon activation through their T cell receptor (TCR) by peptide presentation on major histocompatibility complex class I molecules, naive CD8^{+} T cells undergo clonal expansion and differentiate to diverse phenotypically, functionally, and anatomically distinct effector CD8^{+} T cell subsets (2, 3). The presence of CD8^{+} T cells in the tumor correlates with improved survival in multiple solid malignancies (4); however, these cells often fail to mediate tumor regression (5, 6).

The paradoxical coexistence of intratumoral CD8^{+} T cells and tumor progression indicates that tumors establish immune-privileged microenvironments in patients with advanced cancer (7). Much progress has been made in the last 2 decades in uncovering immune checkpoints in tumor-infiltrating CD8^{+} T cells, which display a spectrum of dysfunctional states induced by persistent TCR stimulation, engagement of inhibitory receptors, the presence of immunosuppressive cell populations and cytokines, and metabolic factors (8). T cell exhaustion is an acquired state of T cell dysfunction, associated with defective proliferative capacities and reduced cytokine production (9), and therapeutic reinvigoration of tumor-specific T cells has uncovered the potential of immunotherapy for diverse tumor types (10, 11).

Authorship note: TY, TH, and TO are co–first authors.

Conflict of interest: The authors have declared that no conflict of interest exists.

Submitted: October 1, 2019
Accepted: March 25, 2020
Published: April 23, 2020.

Reference information: *JCI Insight*. 2020;5(8):e133920. https://doi.org/10.1172/jci.insight.133920.

Although CD8$^+$ T cells with the same epitope specificity can display substantial heterogeneity in chronic viral infection and cancer (12–15), their functions and roles are ill-defined. Mounting evidence has revealed that less-differentiated CD8$^+$ T cells have superior proliferative capacity, longer persistence, and greater antitumor efficacy in vivo compared with fully differentiated effector T cells in the context of adoptive cell therapy (ACT) (12, 13). However, the fate of these less-differentiated tumor-specific CD8$^+$ T cells in the tumor microenvironment (TME) remains unclear, and the relationship between T cell exhaustion and differentiation status has not been clearly delineated.

The present study was prompted by the recent findings that expression of CX3C chemokine receptor 1 (CX3CR1) correlates with the degree of effector CD8$^+$ T cell differentiation and identifies 3 functionally distinct populations of pathogen-specific effector and memory CD8$^+$ T cells in the periphery in infectious models of vaccinia and lymphocytic choriomeningitis virus (16). Here, we set out to elucidate phenotypic and functional heterogeneity of antigen-specific effector CD8$^+$ T cells using a preclinical model of melanoma. Similar to antiviral CD8$^+$ T cells (16), CX3CR1 identified 3 distinct effector CD8$^+$ T cell subsets: CX3CR1 negative, intermediate (int), and high (hi), in blood, spleen, lymph nodes (LNs), and the tumor.

Our study reveals that adoptively transferred antigen-specific CX3CR1$^-$CD8$^+$ T cells generate CX3CR1^{int} and CX3CR1^{hi} subsets in the periphery upon vaccination with the cognate antigen, gp100, and CD40/TLR7 stimulation. Expression of coinhibitory receptors, cytokine production and cytolytic capacity, and response to immune checkpoint blockade were different among 3 subsets of CD8$^+$ tumor-infiltrating lymphocytes (TILs). In vivo antitumor reactivity of the CX3CR1^{hi} subset that exhibited potent cytolytic capacity and lower levels of coinhibitory receptors in the tumor was evaluated by a potentially novel mouse model where CX3CR1^{hi}CD8$^+$ T cells can be selectively depleted in vivo using diphtheria toxin (DT). Last, differential impact of PD-L1 blockade on 3 subsets of CD8$^+$ TILs was determined.

Results

CX3CR1 expression levels identify 3 phenotypically distinct subsets of adoptively transferred tumor-specific CD8$^+$ T cells in vivo. CD8$^+$ TILs comprise heterogeneous cell populations with unique differentiation and functional states (8, 9). To elucidate heterogeneity of CD8$^+$ T cells recognizing the same antigen in the TME, we used Pmel-1 TCR-transgenic CD8$^+$ T cells specific for the gp100 melanocyte differentiation antigen expressed on B16 melanomas (17). Pmel-1 T cells were activated with human (h) gp100 peptide, IL-7, and IL-15 for 6 days in vitro (18). These in vitro–activated Pmel-1 T cells have increased fluorescence intensity of CD27 and CD44 compared with T cells before activation but do not express CX3CR1 (Figure 1A and Supplemental Figure 1A; supplemental material available online with this article; https://doi.org/10.1172/jci.insight.133920DS1). These less-differentiated Pmel-1 T cells were adoptively transferred to mice with large established s.c. B16 melanomas (Figure 1B). Mice received 500 cGy of sublethal irradiation prior to ACT for lymphodepletion. To maximize antitumor efficacy of adoptively transferred T cells, mice received vaccination with hgp100, agonistic CD40 antibody (Ab), and TLR7 agonist and systemic administration of IL-2 (18, 19). Adoptively transferred T cells expressing CD90.1 can be distinguished from endogenous T cells (CD90.2) in C57BL/6 mice. Blood, spleen, LNs, and tumors were harvested at different time points for phenotypic and/or functional analysis of infused Pmel-1 T cells.

Adoptively transferred Pmel-1 T cells started to express CX3CR1 4 days after infusion, and 3 distinct CX3CR1$^-$, CX3CR1^{int}, and CX3CR1^{hi} subsets of CD8$^+$CD90.1$^+$ T cells were identified in blood, spleen, LNs, and the tumor by day 7 (Figure 1C and Supplemental Figure 1B). The frequency of the CX3CR1^{int} subset was maintained in the tumor compared with other tissues whereas CX3CR1$^-$ and CX3CR1^{hi} subsets became dominant in LNs and blood on day 25, respectively (Figure 1C).

Next, we performed phenotypic analysis of 3 subsets of Pmel-1 T cells in spleen and the tumor. In both spleen and the tumor, the CX3CR1$^-$ subset contained more CD62L$^+$, CD127$^+$, and KLRG1$^-$ populations, suggesting less-differentiated T cells while the CX3CR1^{hi} subset comprised more CD62L$^-$, CD127$^-$, and KLRG1$^+$ populations consistent with terminally differentiated effector T cells (Figure 1D) (12, 20, 21). Transcription factor T cell factor 1 (Tcf1), encoded by *Tcf7*, is a critical regulator of T cell development and memory formation (22–25). Emergent evidence indicates that intratumor Tcf1$^+$CD8$^+$ T cells have increased self-renewal, expansion, and differentiation capacity and play an important role in controlling tumor growth (26–30). We examined Tcf1 expression in the 3 subsets of tumor-infiltrating Pmel-1 CD8$^+$ T cells and found that the CXC3R1$^-$ subset expressed significantly higher levels of Tcf1 compared with CXC3R1^{int} and CXC3R1^{hi} subsets (Figure 1E). Of note, we did not observe the expression of a type I transmembrane gly-

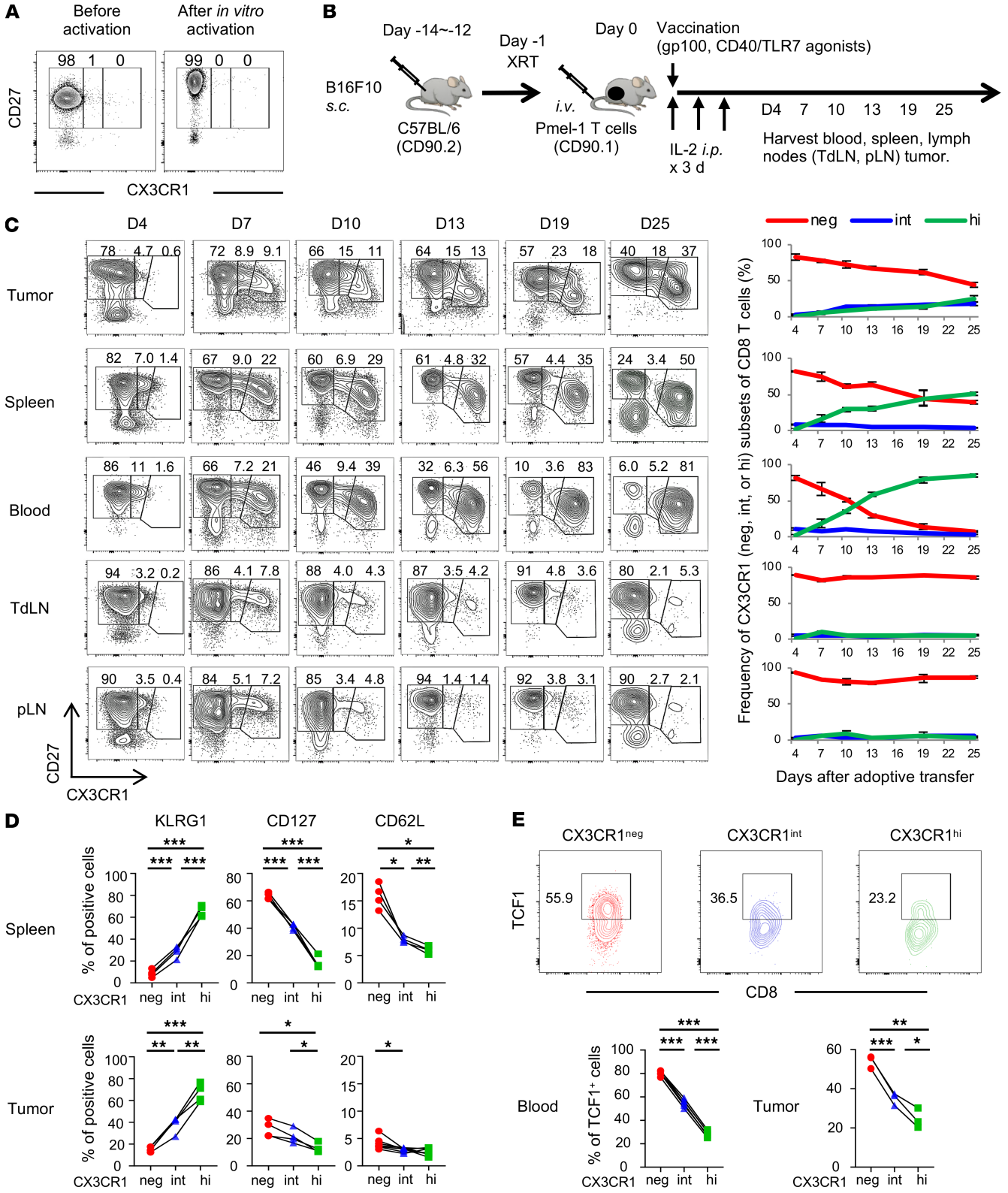

Figure 1. CX3CR1 expression levels identify 3 phenotypically distinct subsets of adoptively transferred tumor-specific CD8⁺ T cells. (**A**) Phenotypic analysis of Pmel-1 T cells before and after in vitro activation. (**B**) Experimental protocol. XRT, external beam radiation therapy. (**C**–**E**) Phenotypic analysis of Pmel-1 CD8⁺CD90.1⁺ T cells adoptively transferred into C57BL/6 mice (CD90.2) bearing B16 tumors. TdLN, tumor-draining lymph nodes; pLN, nondraining peripheral lymph nodes. (**C**) Left shows representative FACS plots gated with the CD8⁺CD90.1⁺ population. Right shows kinetics and frequency of each T cell subset based on CX3CR1 expression. Mean (±SEM). (**D**) Phenotype of 3 subsets of Pmel-1 T cells in spleens (upper) and tumors (lower) determined by CX3CR1 expression on day 7. KLRG1, killer cell lectin like receptor G1. (**E**) Representative FACS plots showing TCF1 expression in each subset of Pmel-1 CD8⁺ TILs determined by CX3CR1 expression on day 7. The lower panels show frequency of TCF1⁺ cells in peripheral blood and B16 tumors in mice treated with ACT. (**C**–**E**) (n = 3–7 mice per group); $^*P < 0.05$, $^{**}P < 0.01$, and $^{***}P < 0.005$ by 1-way ANOVA test with Tukey's multiple comparisons. See also Supplemental Figure 1.

coprotein CD101 in tumor-infiltrating Pmel-1 CD8$^+$ T cells (Supplemental Figure 1C), which was recently identified in the terminally differentiated state of CD8$^+$ T cells in chronic viral infection (31).

Expression of coinhibitory receptors on 3 subsets of CD8$^+$ TILs inversely correlated with the degree of T cell differentiation defined by CX3CR1. To elucidate the exhaustion state of 3 subsets of intratumor CD8$^+$ T cells with the same epitope specificity, we evaluated expression of coinhibitory receptors on Pmel-1 T cells in B16 melanoma. Interestingly, programmed cell death 1 (PD-1) expression on tumor-infiltrating Pmel-1 T cells inversely correlated with the degree of differentiation defined by CX3CR1 (Figure 2A). Furthermore, despite their terminally differentiated status, the CX3CR1^{hi} subset expressed significantly lower levels of coinhibitory receptors, PD-1, LAG-3, and TIGIT in the tumor compared with CX3CR1$^-$ and CX3CR1^{int} subsets (Figure 2A). We evaluated kinetics of coinhibitory receptor expression on intratumor Pmel-1 T cells at 7, 10, 13, and 19 days after ACT. This revealed that the CX3CR1^{hi} subset persistently expressed significantly lower levels of coinhibitory receptors (Figure 2, B–D). Of note, these coinhibitory receptors were not expressed on Pmel-1 T cells in the blood, spleen, or LNs (data not shown).

We also profiled expression of coinhibitory receptors on 3 subsets of CD8$^+$ T cells infiltrating human melanoma tumors. Consistent with Pmel-1 T cells in B16 tumors, PD-1 expression on human melanoma-infiltrating CD8$^+$ T cells inversely correlated with CX3CR1 expression (Figure 3 and Supplemental Figure 2). Furthermore, CX3CR1^{hi}CD8$^+$ T cells in human melanoma expressed significantly lower levels of coinhibitory receptors, PD-1, LAG-3, TIM-3, and 2B4 compared with CX3CR1$^-$ and CX3CR1^{int} subsets (Figure 3).

Functional heterogeneity of 3 subsets of tumor-infiltrating antigen-specific CD8$^+$ T cells defined by CX3CR1. Functional heterogeneity of CD8$^+$ TILs in the context of differentiation status remains elusive. To this end, we harvested splenocytes and TILs 7 days after ACT, cocultured them with hgp100 peptide, and evaluated intracellular expression of IL-2, IFN-γ, TNF-α, granzyme B (GZMB), and granzyme A (GZMA) in Pmel-1 T cells. We found the CX3CR1$^-$ subset in spleen contained more cytokine-producing CD8$^+$ T cells compared with CX3CR1^{int} and CX3CR1^{hi} subsets (Figure 4A), consistent with observations from infectious models evaluating 3 subsets of virus-specific CD8$^+$ T cells defined by CX3CR1 (16). In the tumor, however, we observed a dramatic reduction in the number of cytokine-producing CX3CR1$^-$ cells, and the CX3CR1^{int} subset was found to contain more polyfunctional cells producing IL-2, IFN-γ, and TNF-α compared with CX3CR1$^-$ and CX3CR1^{hi} subsets (Figure 4A). Both in spleen and the tumor, expression of GZMA correlated with T cell differentiation status whereas no difference in GZMB expression was found among all 3 Pmel-1 T cell subsets (Figure 4A).

Although these results provide insight into the functional heterogeneity among 3 subsets in the periphery and the tumor, cytokines from 1 subset might affect function of the other subsets during coculture with hgp100 peptide. To evaluate functional exhaustion of 3 subsets of tumor-infiltrating effector CD8$^+$ T cells compared with their peripheral counterparts, we flow-isolated each subset of splenic and intratumor effector (CD44$^+$CD62L$^-$) CD8$^+$CD90.1$^+$ T cells, cocultured them with B16 melanoma cells, and measured cytokine production by ELISA. We found production of effector cytokines, IL-2, IFN-γ, and TNF-α against B16 melanomas was severely impaired in the CX3CR1$^-$ subset while cytokine production from intratumor CX3CR1^{int} and CX3CR1^{hi} subsets was relatively preserved compared with their splenic counterparts (Figure 4B).

Next, to evaluate the cytolytic activity of 3 subsets of CD8$^+$ T cells, we cocultured and flow-isolated each subset of tumor-infiltrating Pmel-1 T cells with luciferase-transfected B16 melanoma cells. As measured using a bioluminescence-based cytotoxicity assay, CX3CR1^{hi}CD8$^+$ TILs exhibited significantly higher cytotoxicity than CX3CR1$^-$ and CX3CR1^{int} subsets (Figure 4C). Furthermore, real-time reverse transcription PCR (real-time RT-PCR) analysis showed *Gzma*, *Gzmb*, *Gzmk*, and perforin (*Prf1*) were enriched in the CX3CR1^{hi} subset compared with CX3CR1$^-$ and CX3CR1^{int} subsets (Figure 4D). Consistent with these results, we found increased perforin, GZMA, GZMB, and GZMK expression on CX3CR1^{hi} TILs from a patient with melanoma (Figure 4E).

In vivo antitumor efficacy of antigen-specific CX3CR1^{hi}CD8$^+$ T cells after ACT. Based on analysis of adoptively transferred Pmel-1 CD8$^+$ T cells, we have thus far shown 3 phenotypically and functionally distinct antigen-specific effector CD8$^+$ T cell subsets in the tumor: (a) the CX3CR1$^-$ subset that represents less-differentiated CD8$^+$ T cells with significantly higher coinhibitory receptors and Tcf1 but severely impaired effector function in the TME, (b) the CX3CR1^{int} subset that also expresses high levels of coinhibitory receptors but have relatively preserved cytokine production capacity in the tumor, and (c) the terminally differentiated

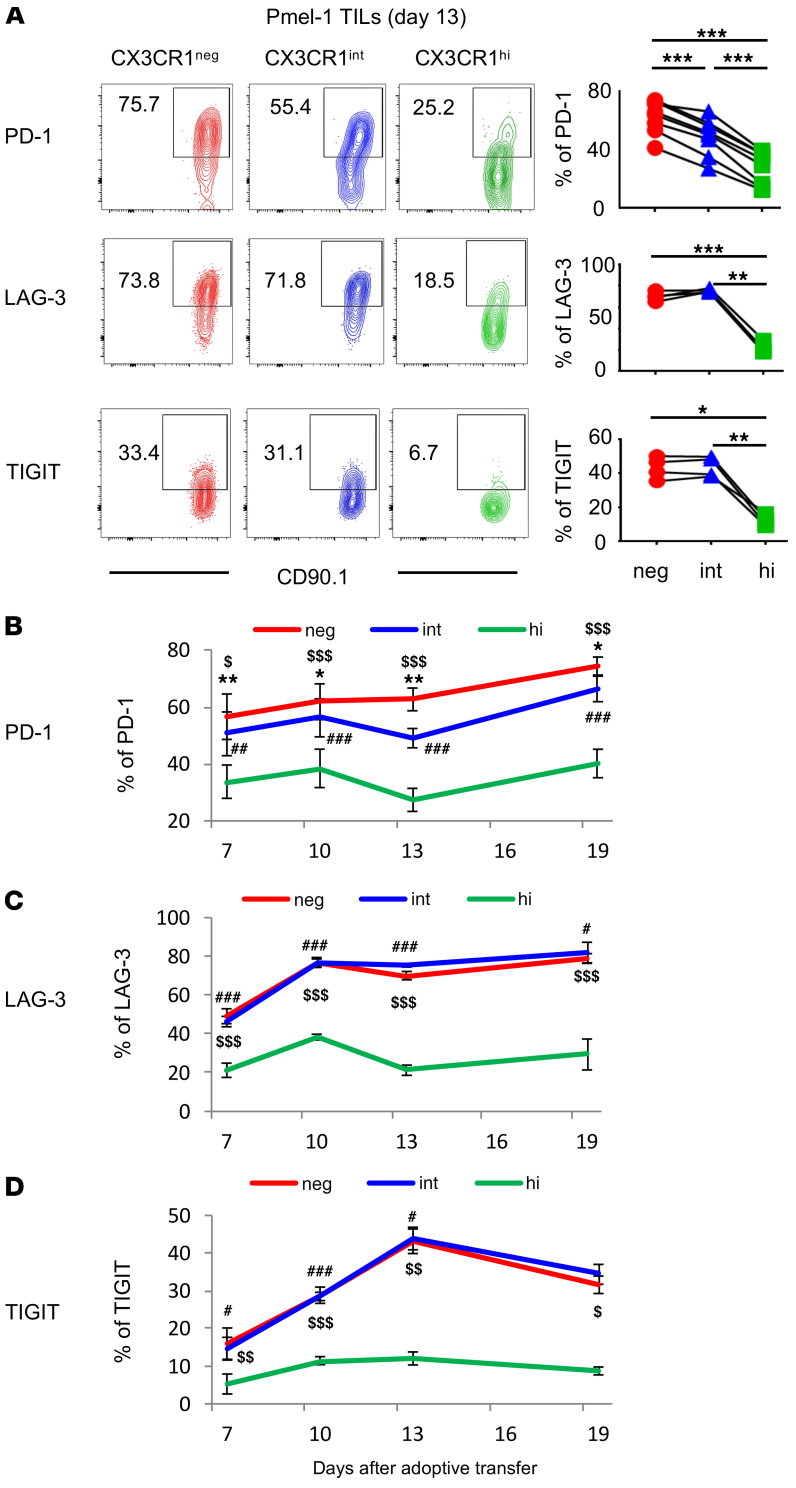

Figure 2. Tumor-infiltrating CX3CR1^{hi}CD8^{+} T cells express significantly lower levels of coinhibitory receptors despite their terminally differentiated status. (**A**) Phenotypic analysis of Pmel-1 CD8^{+} tumor-infiltrating lymphocytes (TILs) 13 days after adoptive cell transfer. Left shows representative FACS plots of each subset of Pmel-1 CD8^{+} TILs determined by CX3CR1 expression. Right shows percentage of each subset from a group. (n = 4–7 mice per group.) LAG-3, lymphocyte-activation protein 3; TIGIT, T cell immunoreceptor with Ig and ITIM domains. (**B**–**D**) Kinetic analysis of Pmel-1 CD8^{+} T cells adoptively transferred into C57BL/6 recipients bearing B16 tumors. Data show percentage of PD-1, LAG-3, TIGIT-expressing CX3CR1–, CX3CR1^{int}, and CX3CR1^{hi} Pmel-1 CD8^{+} TILs. (n = 4 mice per group.) (**A**) $^{*}P < 0.05$, $^{**}P < 0.01$, and $^{***}P < 0.005$. (**B**–**D**) Mean (±SEM). $^{*}P < 0.05$, $^{**}P < 0.01$, and $^{***}P < 0.005$ CX3CR1^{-} vs. CX3CR1^{int}; $^{\#}P < 0.05$, $^{\#\#}P < 0.01$, and $^{\#\#\#}P < 0.005$ CX3CR1^{int} vs. CX3CR1^{hi}; $^{\$}P < 0.05$, $^{\$\$}P < 0.01$, and $^{\$\$\$}P < 0.005$ CX3CR1^{-} vs. CX3CR1^{hi} by 1-way ANOVA test with Tukey's multiple comparisons.

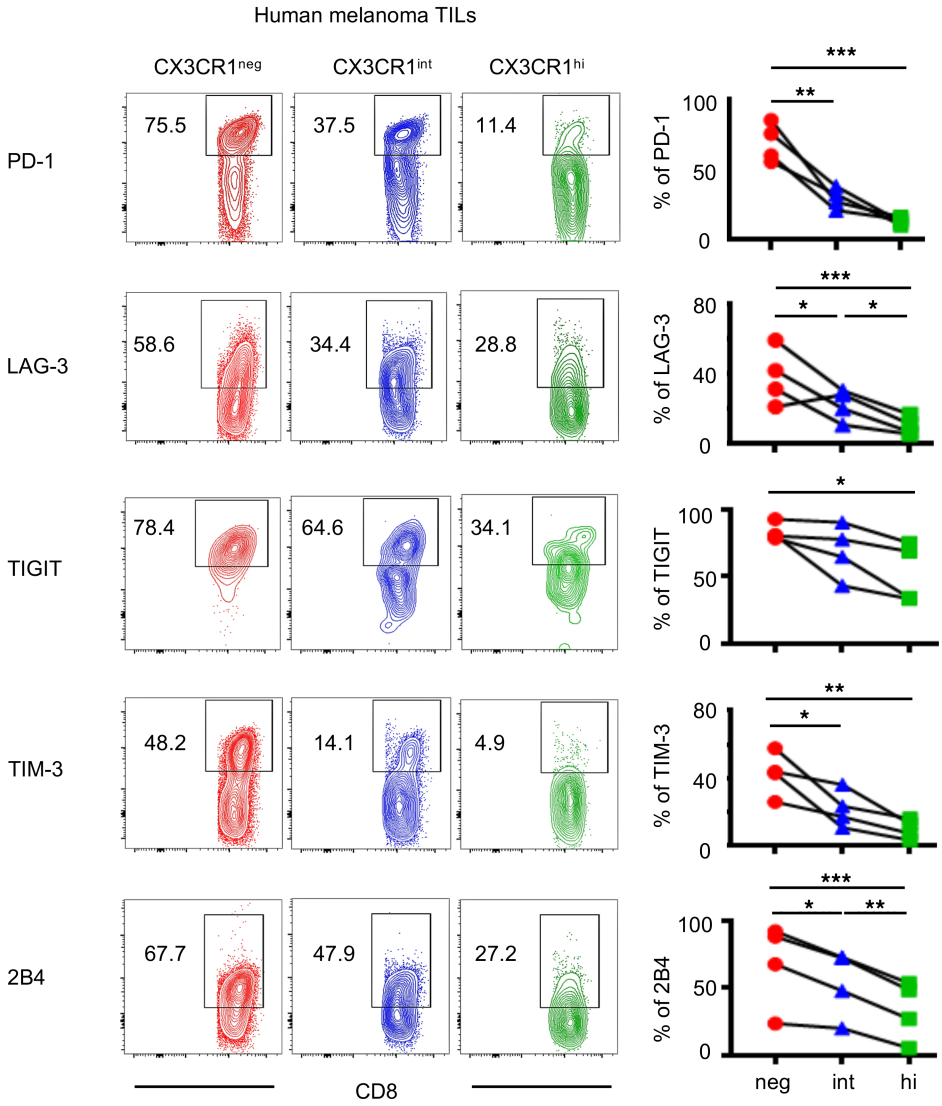

Figure 3. Human tumor-infiltrating CX3CR1^{hi}CD8^{+} T cells express low levels of coinhibitory receptors. Phenotypic analysis of human melanoma CD8^{+} TILs. Right shows percentages of each subset of CD8^{+} TILs determined by CX3CR1 expression. (n = 4 per group.) *P < 0.05, **P < 0.01, and ***P < 0.005 by 1-way ANOVA test with Tukey's multiple comparisons. See also Supplemental Figure 2. TIM-3, T cell Ig and mucin-domain containing-3.

CX3CR1^{hi} subset that expresses significantly higher levels of KLRG1, but lower levels of coinhibitory receptors and Tcf1, and exhibits robust cytotoxicity. Of these 3 subsets, CX3CR1^{hi}CD8^{+} T cells were found to be a unique subset that might be affected less by inhibitory signals compared with CX3CR1^{-} and CX3CR1^{int} subsets in the TME and able to mediate potent cytotoxicity against tumors in vivo.

Previous preclinical studies indicated decreased antitumor responses in CX3CR1$^{-/-}$ mice (32, 33) and a critical role of the CX3CR1/CX3CL1 pathway in T cell/NK cell–mediated antitumor immunity (34–36); however, these studies did not distinguish antitumor efficacy between phenotypically and functionally distinct CX3CR1^{int} and CX3CR1^{hi} subsets. Moreover, CX3CR1 is expressed not only on T cells but also on monocytes, dendritic cells (DCs), γδ T cells, and NK cells (37). Therefore, we sought to generate a mouse model where we could selectively deplete tumor antigen-specific CX3CR1^{hi}CD8^{+} T cells in vivo.

Diehl et al. developed inducible CX3CR1–diphtheria toxin receptor (DTR) mice by introducing a *loxP*-floxed stop cassette followed by DTR into the *Cx3cr1* locus (38). In their study, CX3CR1-DTR mice were crossed to CD11c-Cre mice, allowing deletion of the stop cassette in CD11c^{+} cells and induction of DTR in CX3CR1^{+} cells. They showed expression of CD11c-Cre excises the stop cassette, allowing for DTR expression and selective depletion of CX3CR1^{hi}CD11c^{+} cells upon administration of DT, with no effect on CX3CR1^{int}CD11c^{+} cells (38).

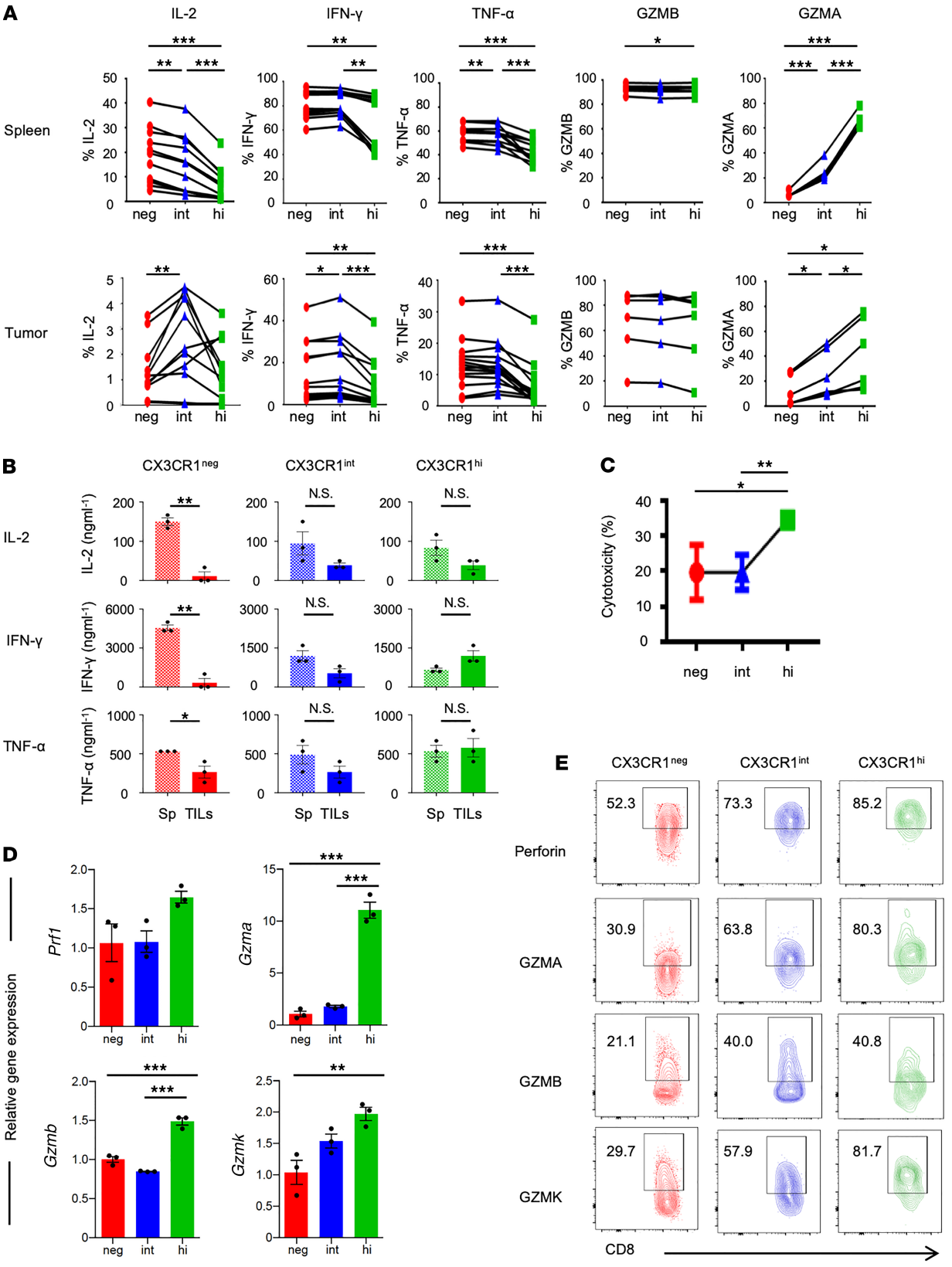

Figure 4. Functional heterogeneity of 3 subsets of tumor-infiltrating antigen-specific CD8⁺ T cells defined by CX3CR1. (**A**) Intracellular production of cytokines against hgp100 peptide and granzymes by Pmel-1 T cells in spleen (upper) and the tumor (lower) 7 days after adoptive transfer. Ex vivo production of cytokines and granzymes shown in the panel are calculated based on the percentages of positive cells. $n = 2$ experiments pooled. $^{*}P < 0.05$, $^{**}P < 0.01$, and $^{***}P < 0.005$ by 1-way ANOVA test with Tukey's multiple comparisons. $n = 2$ experiments pooled. (**B**–**D**) Analysis of 3 flow cytometry–sorted subsets of Pmel-1 effector ($CD44^{+}CD62L^{-}$) $CD8^{+}CD90.1^{+}$ T cells ex vivo cocultured with B16 melanoma cells. (**B**) ELISA showing cytokine production from

supernatants of B16 cocultures either with T cells from spleens (Sp) or TILs of adoptive cell–transferred mice. Mean (±SEM). *$P < 0.05$, **$P < 0.001$, and N.S., not significant by unpaired 2-tailed *t* test. (**C**) Firefly luciferase–based cytotoxicity assay showing hgp100-specific cytotoxicity of each sorted CX3CR1 subset. Mean (±SEM). *$P < 0.05$, and **$P < 0.01$ by unpaired 2-tailed *t* test. (**D**) Quantification of mRNA levels on each flow-sorted CX3CR1 subset during the cocultures. Normalization was done with mouse Thy1.1 gene, which is not expressed on B16 cells. Mean (±SEM). *$P < 0.05$, **$P < 0.01$, and ***$P < 0.005$ by 1-way ANOVA with Tukey's test. (**E**) Phenotypic analysis of human melanoma CD8$^+$ TILs. Numbers indicate cytokine expression on each subset of CD8$^+$ TILs determined by CX3CR1 expression.

To determine in vivo antitumor efficacy of the Pmel-1 CX3CR1^{hi}CD8$^+$ T cell subset, we crossed Pmel-1 mice with CD2-Cre mice (39), followed by CX3CR1-DTR mice (38), and generated Pmel-1 *Cd2-cre/Cx3cr1*$^{+/DTR}$ mice. Expression of *Cd2-cre* excises the *loxP*-floxed stop cassette upstream of the DTR-coding region, allowing for DTR expression and selective depletion of the Pmel-1 CX3CR1^{hi}CD8$^+$ T cell subset upon administration of DT, with no effect on Pmel-1 CX3CR1$^-$ or CX3CR1^{int} cells (Figure 5, A and B).

B16 tumor–bearing mice were treated with adoptive transfer of in vitro–activated Pmel-1 *Cd2-cre/Cx3cr1*$^{+/DTR}$ CD8$^+$ T cells followed by vaccination and IL-2. These mice received phosphate-buffered saline or DT injection every other day for 12 days starting 1 day before ACT (Figure 5A). Adoptive transfer of Pmel-1 *Cd2-cre/Cx3cr1*$^{+/DTR}$ CD8$^+$ T cells significantly delayed tumor growth and increased survival; however, depletion of Pmel-1 CX3CR1^{hi}CD8$^+$ T cells did not alter antitumor efficacy of ACT (Figure 5C).

Response of CX3CR1$^-$, CX3CR1^{int}, and CX3CR1^{hi} CD8$^+$ T cells to antigenic rechallenge. To gain further insight into the antitumor efficacy of 3 subsets of CD8$^+$ T cells, we sorted CX3CR1$^-$, CX3CR1^{int}, and CX3CR1^{hi} subsets from blood and spleen of B16 tumor–bearing mice treated with adoptive transfer of Pmel-1 T cells and restimulated with the gp100 antigen in vitro (Figure 6A). The isolated CX3CR1$^-$ subset expressed significantly higher levels of *Tcf7* and expanded vigorously upon secondary antigenic encounter, compared with CX3CR1^{int} and CX3CR1^{hi} subsets (Figure 6, B and C). Accordingly, isolated CX3CR1$^-$ cells revealed superior proliferative capability in vivo compared with CX3CR1$^+$ (CX3CR1^{int} and CX3CR1^{hi}) subsets upon second adoptive transfer into B16 tumor–bearing mice (Figure 6, D and E). Notably, CX3CR1 expression was stable in the infused CX3CR1$^+$ subsets while CX3CR1$^-$ cells gave rise to CX3CR1$^+$ subsets in vivo (Figure 6F), demonstrating that antigen rechallenge of effector CD8$^+$ T cells reinvokes a unidirectional differentiation program, consistent with observations using virus-specific CD8$^+$ T cells (16). Importantly, adoptively transferred CX3CR1$^-$ but not CX3CR1$^+$ cells significantly delayed tumor growth and increased survival (Figure 6G). Taken together, the CX3CR1$^-$ subset is composed of less-differentiated *Tcf7*$^+$CD8$^+$ T cells that maintain proliferative and differentiation capacity and mediate antitumor efficacy upon antigenic rechallenge.

Less-differentiated CD8$^+$ T cells are preferentially rescued by programmed cell death ligand 1 blockade in the tumor. Although the blockade of immune checkpoints, such as PD-1/programmed cell death ligand 1 (PD-1/PD-L1), reinvigorates tumor-specific CD8$^+$ T cells and can durably control advanced solid malignancies (10), less is known regarding how it works on heterogeneous CD8$^+$ TILs. Evidence from chronic viral infection models suggests that there are differential responses to PD-1/PD-L1 blockade between exhausted CD8$^+$ T cell subpopulations that are characterized by the level of PD-1 expression (40). Our results of different levels of PD-1 expression in CX3CR1$^-$, CX3CR1^{int}, and CX3CR1^{hi} CD8$^+$ T cells indicate the potential of reinvigoration by PD-1/PD-L1 blockade differs among the 3 subsets of CD8$^+$ TILs.

To evaluate the differential impact of PD-L1 blockade on the 3 subsets of tumor-infiltrating CD8$^+$ T cells, we treated B16 tumor–bearing mice with anti–PD-L1 Ab or isotype control Ab after adoptive transfer of Pmel-1 T cells, vaccination, and IL-2 (Figure 7A). PD-L1 blockade caused a significant delay in tumor growth and improved survival in combination with adoptive transfer of Pmel-1 CD8$^+$ T cells while PD-L1 blockade alone had no therapeutic effect (Figure 7B). Although there were no changes in terms of the ratios of each CX3CR1 (neg/int/hi) subset, anti–PD-L1 therapy significantly increased the Ki-67–expressing CX3CR1$^-$CD8$^+$ T subset (Figure 7, C and D). To determine functional reinvigoration of the 3 subsets of CD8$^+$ TILs, we isolated Pmel-1 TILs 7 days after adoptive transfer, cocultured them with hgp100 peptide, and evaluated intracellular expression of effector cytokines, IL-2, TNF-α, IFN-γ, and CD107a. Although we found levels of IL-2, TNF-α, IFN-γ, and CD107a improved in all 3 subsets, a greater impact of PD-L1 blockade was seen on less-differentiated CX3CR1$^-$CD8$^+$ T cell subsets (Figure 7E).

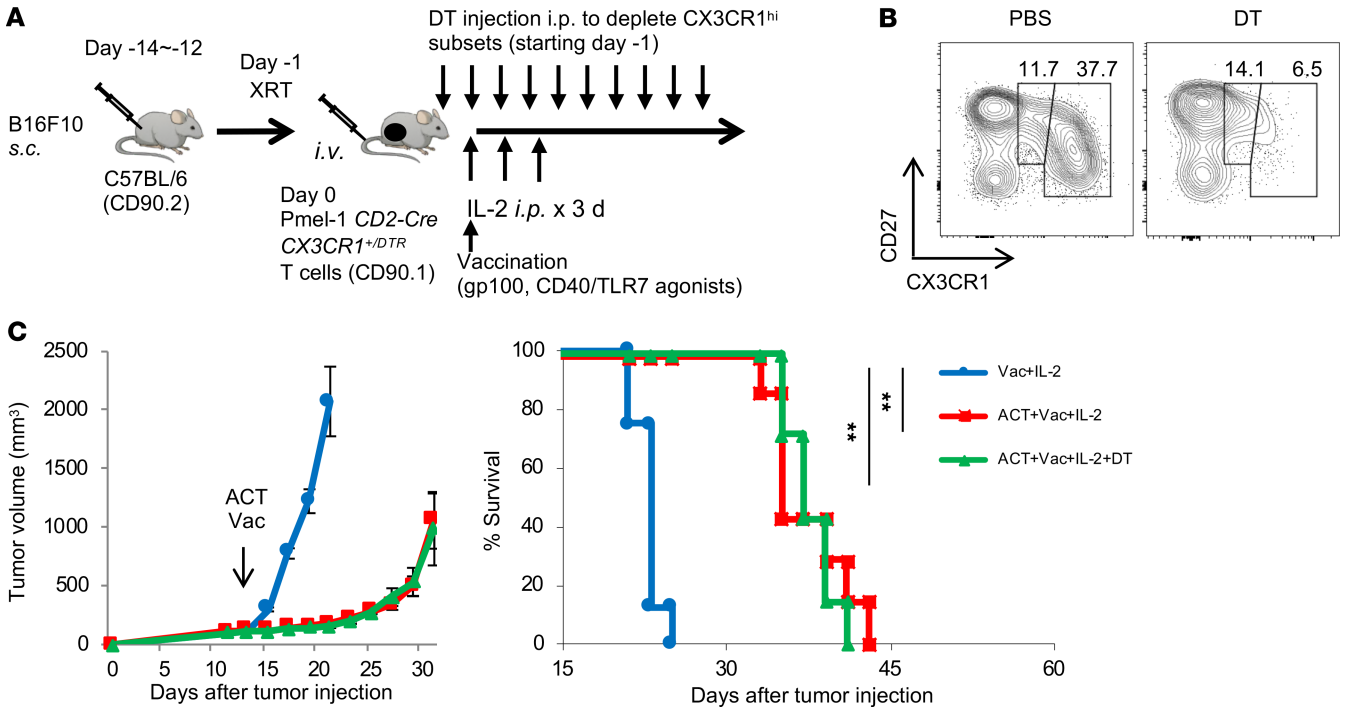

Figure 5. In vivo antitumor efficacy of antigen-specific CX3CR1^{hi}CD8$^+$ T cells after ACT. (**A**) Schematic illustration showing evaluation of in vivo antitumor efficacy of the CX3CR1^{hi} subset using adoptive transfer of Pmel-1 *Cd2-cre/Cx3cr1*$^{+/DTR}$ CD8$^+$ T cells, vaccination, and IL-2 followed by DT administration. (**B**) Representative FACS plots showing selective depletion of the CX3CR1^{hi} subset in peripheral blood upon DT injection in C57BL/6 mice adoptively transferred with Pmel-1 *Cd2-cre/Cx3cr1*$^{+/DTR}$ CD8$^+$ T cells. Expression of CD27 and CX3CR1 on infused Pmel-1 *Cd2-cre/Cx3cr1*$^{+/DTR}$ T cells with or without DT are shown. (**C**) Tumor growth curves and survival curves of C57BL/6 mice bearing B16 melanomas established for 12 days in different treatment groups. ($n \geq 7$ mice per group.) $^{**}P < 0.01$ by log-rank test.

Discussion

The blockade of immune checkpoint molecules, such as PD-1, PD-L1, and cytotoxic T lymphocyte associated protein 4, to unleash T cell–mediated antitumor immunity has demonstrated unprecedented success for the treatment of a variety of malignancies; however, only a minority of patients receive durable clinical benefit (10, 11). Although the targets of immune checkpoint blockade are defined, how it works remains incompletely understood. Elucidating the phenotypic and functional heterogeneity of CD8$^+$ TILs might lead to the development of more efficacious immunotherapies against cancers. The TME comprises effector CD8$^+$ T cells with various states of dysfunction and differentiation, and the relationship between T cell exhaustion and differentiation status has not been defined clearly. In the present study, we sought to delineate phenotypic and functional heterogeneity of CD8$^+$ TILs recognizing the same antigen and the relationship between T cell exhaustion and the differentiation status using a marker of T cell differentiation, CX3CR1 (16, 41, 42).

In a preclinical model of melanoma, we have shown that adoptively transferred antigen-specific CD8$^+$ T cells mediate effective regression of a large established tumor and generate heterogeneous cell populations with unique differentiation states defined by the chemokine receptor CX3CR1. The less-differentiated CX3CR1$^-$ subset in spleen contained the most polyfunctional cells that produced IL-2, IFN-γ, and TNF-α, in line with a recent study using viral infection models (16); however, we found this subset expressed significantly higher levels of coinhibitory receptors in murine and human melanomas. In contrast, the tumor-infiltrating CX3CR1^{hi}CD8$^+$ T cell subset expressed significantly lower levels of coinhibitory receptors. Direct comparison of the 3 subsets of Pmel-1 T cells in spleen and the tumor further demonstrated the intratumor CX3CR1$^-$ subset exhibited severely impaired production of these cytokines compared with their counterparts in spleen while there was no difference in cytokine production from the CX3CR1$^+$ subsets in spleen and the tumor.

Although findings of markedly lower expression of coinhibitory receptors and potent cytotoxicity of the intratumor CX3CR1^{hi} subset are intriguing, our data showed this subset expressed reduced levels of

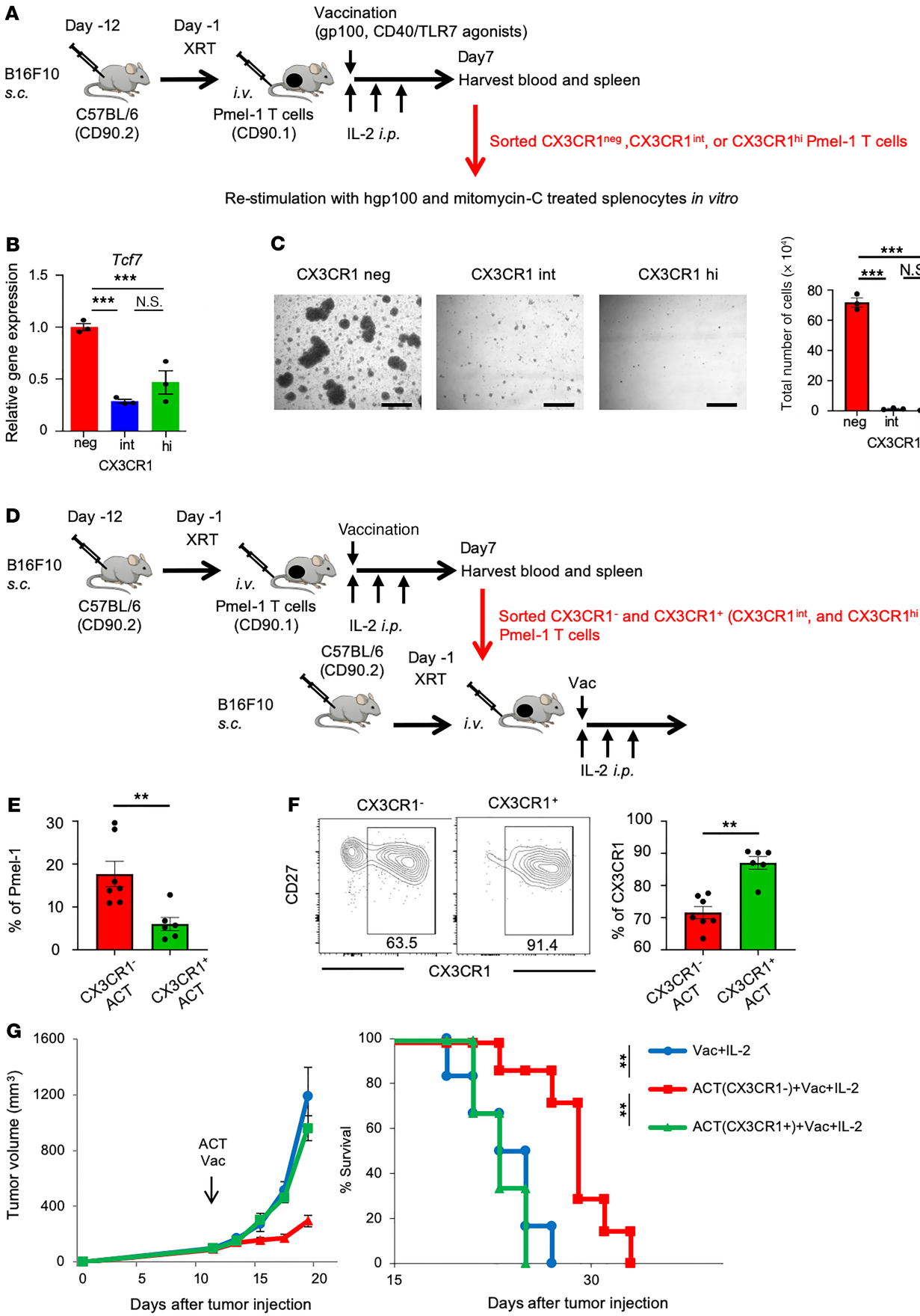
A
Day -12
Day -1
XRT
Vaccination
(gp100, CD40/TLR7 agonists)
Day7
Harvest blood and spleen
B16F10
s.c.
C57BL/6
(CD90.2)
i.v.
Pmel-1 T cells
(CD90.1)
IL-2 i.p.
Sorted CX3CR1neg ,CX3CR1int, or CX3CR1hi Pmel-1 T cells
Re-stimulation with hgp100 and mitomycin-C treated splenocytes in vitro
B
Tcf7
Relative gene expression
***
N.S.
neg
int
hi
CX3CR1
C
CX3CR1 neg
CX3CR1 int
CX3CR1 hi
Total number of cells (× 10⁴)
D
Sorted CX3CR1- and CX3CR1+ (CX3CR1int, and CX3CR1hi) Pmel-1 T cells
Vac
E
% of Pmel-1
**
CX3CR1- ACT
CX3CR1+ ACT
F
CX3CR1-
CX3CR1+
CD27
63.5
91.4
CX3CR1
% of CX3CR1
G
Tumor volume (mm³)
ACT
Vac
Days after tumor injection
% Survival
Vac+IL-2
ACT(CX3CR1-)+Vac+IL-2
ACT(CX3CR1+)+Vac+IL-2

Figure 6. In vitro proliferation and in vivo antitumor efficacy of antigen-specific CX3CR1$^+$CD8$^+$ T cells after ACT. (**A**) Schematic illustration showing evaluation of in vitro proliferation of 3 subsets of Pmel-1 T cells determined by CX3CR1 expression. FACS-sorted cells were stimulated with hgp100 peptide with mitomycin-C–treated B6 splenocytes for 4 days. (**B**) *Tcf7* mRNA expression in each subset quantitated by real-time RT-PCR. Gapdh was used as an internal control. Error bars represent the standard error of the value obtained in the experiments performed in triplicate. (**C**) Left shows representative microscopic pictures of each subset at day 4. Scale bar: 250 μm. Right shows total cell numbers after 4 days of stimulation of each subset. Error bars represent the SEM of the value obtained in the experiments performed in triplicate. (**D**) Schematic illustration showing evaluation of in vivo antitumor efficacy of CX3CR1$^-$ and CX3CR1$^+$ subsets using adoptive transfer of each subset sorted from B16 tumor–bearing mice 7 days after adoptive transfer of Pmel-1 T cells. (**E**) Frequency of adoptively transferred Pmel-1 T cells in blood of B16 tumor–bearing mice infused with either CX3CR1$^-$ or CX3CR1$^+$ as indicated. (**F**) Representative dot plot showing CX3CR1 expression of Pmel-1 T cells in blood of B16 tumor–bearing mice. Expression of CD27 and CX3CR1 on infused CX3CR1$^-$CD8$^+$ or CX3CR1$^+$CD8$^+$ T cells are shown. The right panel shows the percentage of CX3CR1 expression in Pmel-1 T cells in different treatments as indicated. (**G**) Tumor growth curves and survival curves in C57BL/6 mice bearing B16 melanomas established for 12 days in different treatment groups. ($n \geq 6$ mice per group.) Mean (±SEM). $^{**}P < 0.01$, and $^{***}P < 0.005$ by 1-way ANOVA with Tukey's test (**B** and **C**), unpaired 2-tailed *t* test (**D–F**), or log-rank test (**G**).

CD127 along with higher levels of KLRG1 and underwent little to no expansion in response to antigen rechallenge. Furthermore, depletion of the CX3CR1^{hi} subset with DT injection did not decrease antitumor efficacy of adoptively transferred Pmel-1 *Cd2-cre/Cx3cr1*$^{+/DTR}$ CD8$^+$ T cells in vivo. These findings were rather unexpected because of the previous studies showing decreased antitumor immunity in CX3CR1$^{-/-}$ mice or with the use of the CX3CR1 antagonist (32–35, 43). A key difference between previous studies and ours, however, is that our model allows us to selectively deplete the antigen-specific CX3CR1^{hi}CD8$^+$ T cell subset and does not affect other immune cells, including monocytes, DCs, γδ T cells, endogenous CD8$^+$ T cells, and NK cells (37), that may express CX3CR1 and contribute to antitumor immunity.

This discrepancy might also be associated with the lack of CX3CL1 expression in a B16 mouse melanoma model (34), where function of CX3CR1 as a chemokine receptor might not play a significant role in antitumor efficacy. Xin et al. reported that intratumor injection of an adenoviral vector expressing mouse fractalkine (CX3CL1) gene into B16 cells significantly suppressed tumor growth in a T cell/NK cell–dependent fashion (34). Other studies using Lewis lung carcinoma also revealed that tumor growth was significantly inhibited by the increased expression of CX3CL1 in the tumor (44, 45), demonstrating a key role of the CX3CR1/CX3CL1 axis in antitumor immunity in CX3CL1-expressing tumors.

Another possibility is that previous studies using CX3CR1$^{-/-}$ mice or a CX3CR1 antagonist affect both CX3CR1^{int}CD8$^+$ and CX3CR1^{hi}CD8$^+$ T cells and cannot distinguish therapeutic efficacy between these 2 functionally distinct subsets, and our results may suggest an important role of CX3CR1^{int}CD8$^+$ T cells in antitumor T cell immunity. We found that the CX3CR1^{int} subset showed characteristics of memory and effector T cells, expressing CD27, CD127, and KLRG1. Moreover, the CX3CR1^{int} subset contained a substantially higher frequency of cytokine-producing cells compared with CX3CR1$^-$CD8$^+$ and CX3CR1^{hi}CD8$^+$ T cell subsets in the tumor. Although antitumor reactivity of the CX3CR1^{int} subset arising in the effector phase remains to be elucidated, 2 previous studies revealed an important role played in the memory phase by antigen-specific CX3CR1^{int}CD8$^+$ T cells in infection models. Gerlach et al. revealed that virus-specific CX3CR1^{int}CD8$^+$ T cells not only possess the highest self-renewal capacity but also are the dominant subset surveying peripheral tissues among all memory T cells (16). In another recent study, it was shown that CX3CR1^{int}CD8$^+$ T cells form a substantial component of the memory pool in response to persistent viruses and vaccines in both mice and humans (42). In line with this, we observed that the frequency of the CX3CR1^{int}CD8$^+$ T cell subsets remained elevated in the tumor but not in blood, spleen, and LNs.

The molecular and cellular mechanisms that regulate CX3CR1$^-$CD8$^+$ T cells to produce CX3CR1$^+$ subsets remain to be elucidated. In our preclinical model of ACT, we found that CD40/TLR7 stimulation facilitated adoptively transferred CX3CR1$^-$CD8$^+$ T cells to generate CX3CR1$^+$ CD8$^+$ T cells, in line with recent reports showing a critical role of CD4$^+$ T cell help or CD40 signaling for the generation of CX3CR1$^+$CD8$^+$ T cells (36, 43). Differentiation of CD8$^+$ T cells from CX3CR1^{int} to CX3CR1^{hi} subsets is unidirectional (16, 42), and CX3CR1 is stably expressed on effector CD8$^+$ T cells, unlike some activation and proliferation markers, such as CD25, CD69, and Ki-67, which are transiently expressed after activation, suggesting potential utility of CX3CR1 on CD8$^+$ T cells as a marker of response to immunotherapy. Indeed, emerging evidence has shown an increased frequency of peripheral blood CX3CR1$^+$CD8$^+$ T cells in patients responding to immune checkpoint blockade (33, 46).

Our experiments using Pmel-1 *Cd2-cre/Cx3cr1*$^{+/DTR}$ CD8$^+$ T cells and second adoptive transfer of sorted CX3CR1$^-$ and CX3CR1$^+$ (CX3CR1^{int} and CX3CR1^{hi}) subsets suggest a critical role of tumor-specific CX3CR1$^-$CD8$^+$ T cells in the context of ACT. This finding is in line with a growing body of evidence

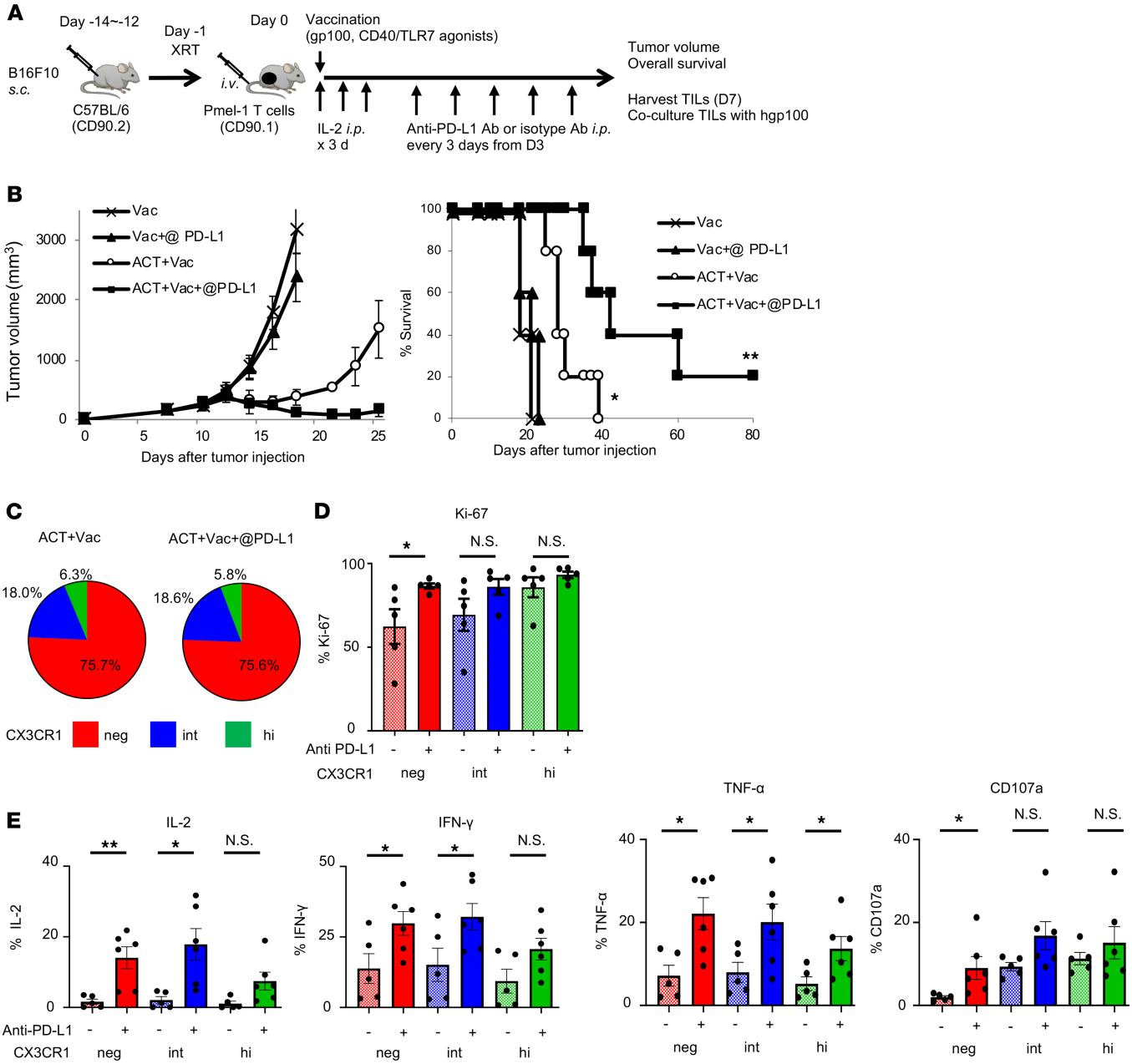

Figure 7. Less-differentiated CX3CR1$^-$CD8$^+$ T cells are preferentially rescued by PD-L1 blockade in the tumor. (**A**) Schematic of combination treatment of ACT with anti–PD-L1 Abs in C57BL/6 mice bearing B16 melanoma. (**B**) Tumor growth curves and survival curves in different treatment groups. (n = 5 mice per group.) Mean (±SEM). *P < 0.009 vs. Vac and Vac + anti–PD-L1 Ab (@ PD-L1), and **P < 0.009 vs. other groups using log-rank (Mantel-Cox) test. (**C** and **D**) Percentage (**C**) and Ki-67$^+$ cells (**D**) of 3 subsets of Pmel-1 CD8$^+$ TILs based on CX3CR1 expression 7 days after ACT. (**E**) Ex vivo production of cytokines (IL-2, IFN-γ, TNF-α, and CD107a) and cytotoxic molecules calculated based on the percentages of positive cells 7 days after ACT. (n = 6 mice per group.) Mean (±SEM). *P < 0.05, **P < 0.01, and N.S., not significant by unpaired 2-tailed t test.

indicating less-differentiated polyfunctional CD8$^+$ T cells capable of producing IL-2, IFN-γ, and TNF-α preferentially survive and provide greater protection in viral infection (47–49) and mediate robust antitumor immunity compared with fully differentiated effector T cells secreting only IFN-γ and/or TNF-α in vivo (12, 13). A potentially novel finding in the current study was that less-differentiated T cells remain the crucial CD8$^+$ T cell subset in mediating effective regression of an established tumor among heterogeneous populations after ACT.

Phenotypic and functional characteristics of T cell exhaustion have been extensively studied in murine models of viral infections and cancer; however, the lineage origin of exhausted CD8$^+$ TILs

remains elusive. Our results are in agreement with a previous study showing that exhausted virus-specific $CD8^+$ T cells arise from the memory precursor $KLRG1^{lo}CD127^{hi}$ subset, rather than from a terminally differentiated $KLRG1^{hi}$ subset of effector $CD8^+$ T cells in a chronic viral infection model (50), and support the notion that T cell exhaustion is not a terminal differentiation, but rather develops progressively over time from a skewed pattern of memory T cell differentiation during chronic stimulation (9, 50, 51). Our findings of a crucial role played by the $CX3CR1^-$ subset expressing Tcf1 in antitumor efficacy also align with recent studies showing importance of $Tcf1^+CD8^+$ T cells with stemlike properties in the setting of chronic infection and cancer (15, 26–30).

Although therapeutic reinvigoration of tumor-specific $CD8^+$ T cells revolutionized treatment for a number of malignancies, gaps in understanding the exact mechanisms that regulate $CD8^+$ T cell responses in the TME remain a major impediment in efforts to improve immunotherapy. We found anti–PD-L1 therapy augments antitumor efficacy of adoptively transferred $CD8^+$ T cells, and the impact of anti–PD-L1 therapy on proliferation and cytokine production was more pronounced in tumor-infiltrating $CX3CR1^-$ $CD8^+$ T cells expressing Tcf1 and PD-1. These findings are in agreement with emergent evidence showing that intratumor $Tcf1^+PD\text{-}1^+CD8^+$ T cells play critical roles in tumor control and respond to anti–PD-1/PD-L1 therapy in mouse models and patients (28, 29). Collectively, these results suggest that PD-L1 blockade improves antitumor efficacy of adoptively transferred $CD8^+$ T cells by preferentially rescuing subsets that are playing a critical role in mediating tumor regression.

In summary, the current study provides insight into the phenotypic and functional heterogeneity of tumor-specific effector $CD8^+$ T cells, identifies distinct subsets exhibiting a high degree of exhaustion and mediating antitumor efficacy in the TME, and suggests differential impact of PD-L1 blockade on 3 subsets of $CD8^+$ TILs defined by CX3CR1.

Methods

Mice. Female C57BL/6 mice were purchased from The Jackson Laboratory. Pmel-1 TCR-transgenic mice [B6.Cg *Thy1*^{a}-Tg(TcraTcrb)8Rest/J)], CD2-Cre mice [C57BL/6-Tg(CD2-cre)1Lov/J] (39), and CX3CR1-DTR mice (B6N.129P2-Cx3cr1$^{tm3(DTR)Litt}$/J) (38) on C57BL/6 background were purchased from The Jackson Laboratory and bred in-house (Roswell Park Comprehensive Cancer Center). For inducible Pmel-1 *Cd2-cre*/*Cx3cr1*$^{+/DTR}$ mice, we first crossed Pmel-1 mice with CD2-Cre mice. Then, Pmel-1$^{+/-}$ *Cd2-cre* mice were backcrossed to Pmel-1 mice to generate Pmel-1$^{+/+}$ *Cd2-cre* mice. Next, Pmel-1$^{+/+}$ *Cd2-cre* mice were crossed with CX3CR1-DTR mice to generate Pmel-1 *Cd2-cre*/*Cx3cr1*$^{+/DTR}$ mice, allowing induction of DTR in Pmel-1 $CX3CR1^{hi}CD8^+$ T cells. For depletion of Pmel-1 $CX3CR1^{hi}CD8^+$ T cells, DT (MilliporeSigma) (500 ng/dose/mouse) was administered intraperitoneally (i.p.) every other day starting from 1 day before adoptive transfer of Pmel-1 *Cd2-cre*/*Cx3cr1*$^{+/DTR}$ $CD8^+$ T cells for 12 days. All mice were 7 to 10 weeks old at the beginning of each experiment and were maintained under specific pathogen–free conditions at the Roswell Park animal facility according to approved institutional guidelines.

Cell lines. The murine B16F10 melanoma cell line was purchased from ATCC. B16F10 cells were cultured in RPMI (Gibco, Thermo Fisher Scientific) supplemented with 10% FBS (MilliporeSigma), 1% nonessential amino acids (Gibco, Thermo Fisher Scientific), 2 mM GlutaMAX-1 (Gibco, Thermo Fisher Scientific), 100 U/mL penicillin-streptomycin (Gibco, Thermo Fisher Scientific), and 55 μM 2-mercaptoethanol (Gibco, Thermo Fisher Scientific). For the generation of mouse B16F10 cell lines with Luciferase, B16F10 cells were infected with lentiviruses encoding Luciferase (pLenti PGK V5-LUC Neo) (w623-2) (Addgene plasmid 21471), a gift from Eric Campeau (University of Massachusetts Medical School, Worcester, Massachusetts, USA) (52), along with lentiviral packaging plasmids psPAX2 and pMD2.G (Addgene plasmids 12260 and 12259, respectively), gifts from Didier Trono (Ecole Polytechnique Fédérale de Lausanne, Lausanne, Switzerland). Cells were authenticated by morphology, phenotype, and growth; routinely screened for mycoplasma; and maintained at 37°C in a humidified 5% CO_2 atmosphere.

Treatment regimens (ACT, vaccination, cytokine administration, and PD-L1 blockade). For ACT, Pmel-1 and Pmel-1 *Cd2-cre*/*Cx3cr1*$^{+/DTR}$ splenocytes were cultured with murine (m) IL-7 (10 ng/mL) and mIL-15 (10 ng/mL; PeproTech) for 6 days in the presence of 1 μM of $hgp100_{25\text{-}33}$ peptide, KVPRNQDWL (GenScript). Female C57BL/6 mice were injected s.c. with 5×10^5 B16F10 cells. Mice were treated 12~14 days later with i.v. adoptive transfer of about 1×10^6 to 3×10^6 in vitro–activated T cells. Mice were injected with 20,000~40,000 IU recombinant human IL-2 (rhIL-2) (Prometheus Laboratories Inc.) i.p. once on the day of vaccination and twice a day on the 2 following days. Mice were also vaccinated with 100 μL of saline containing 100 μg of

Table 1. Fluorochrome-conjugated Abs used in flow cytometry

Ab	Clone	Manufacturer
Human		
CD8	RPA-T8	BD Biosciences
CD27	O323	BioLegend
PD-1	MIH4	Thermo Fisher Scientific
CX3CR1	2A9-1	BD Biosciences
LAG3	3DS223H	Thermo Fisher Scientific
TIGIT	MBSA43	Thermo Fisher Scientific
TIM3	F38-2E2	BioLegend
2B4	C1.7	BioLegend
GZMA	GzA-3G8.5	Thermo Fisher Scientific
GZMB	GB11	BioLegend
GZMK	G3H69	BD Biosciences
Perforin	dG9	BioLegend
Mouse		
CD8	53-6.7	BioLegend
CD90.1	OX-7	BioLegend
CX3CR1	SA011F11	BioLegend
CD27	LG.7F9	Thermo Fisher Scientific
KLRG1	2F1	BioLegend
CD127	A7R34	BioLegend
CD122	TM-β1	BioLegend
CD44	IM7	BioLegend
CD62L	MEL-14	BioLegend
Tim3	8B.2C12	Thermo Fisher Scientific
CD160	7H1	BioLegend
TRAIL	N2B2	BioLegend
Lag3	631501	R&D Systems, Bio-Techne
Tigit	VSIG9	BioLegend
CD101	Moushi101	Thermo Fisher Scientific
TCF1	S33-966	BD Biosciences
IFN-γ	XMG1.2	BD Biosciences
IL2	JES6-5H4	BioLegend
TNF-α	MP6-XT22	BD Biosciences
GZMA	GzA-3G8.5	Thermo Fisher Scientific
GZMB	16G6	Thermo Fisher Scientific

hgp100 peptide, 50 μg of CD40-specific Ab (clone FGK4.5, Bio X Cell), and 50 mg of imiquimod cream 5% (Perrigo) applied on the vaccination sites after adoptive transfer as described before (18). In some experiments treated mice received 500 cGy of sublethal irradiation prior to ACT to mimic the lymphodepletion done in current clinical ACT protocols (53). For the second ACT experiment, blood and splenocytes were harvested from ACT-treated, B16-bearing, female C57BL/6 mice 7 days after adoptive transfer of Pmel-1 T cells. After $CD8^+$ cells' isolation with CD8a microbeads (Ly-2, Miltenyi Biotech) according to the manufacturer's protocol, Pmel-1 T cells were identified with CD90.1 positivity and then sorted into 2 populations according to CX3CR1 expression with SONY MA900. Next, 1×10^6 sorted $CX3CR1^-$ and $CX3CR1^+$ cells were adoptively transferred into B16-bearing, female C57BL/6 mice followed by IL-2 and vaccination as above. For PD-L1 blockade, anti–PD-L1 Ab (10F.9G2, Bio X Cell) or rat IgG2b Ab (LTF-2, Bio X Cell) were given i.p. every third day from 3 days after ACT at a dose of 200 μg/mouse. Tumor volumes were calculated by determining the length of long (L) and short (S) diameters, where volume = (L × S × S)/2. Experimental endpoints were reached when tumors exceeded 20 mm in diameter or when mice became moribund and showed signs of lateral recumbency, cachexia, lack of response to noxious stimuli, or observable weight loss.

Flow cytometry and intracellular granzymes, IL-2, IFN-γ, and TNF-α assays. Fluorochrome-conjugated Abs are shown in Table 1. DAPI, LIVE/DEAD Fixable Aqua (Thermo Fisher Scientific), or LIVE/DEAD Fixable Near-IR Dead Cell Stain Kit (Thermo Fisher Scientific) staining cells were excluded from analysis. Intracellular

Table 2. Primer sequences used in real-time RT-PCR analysis

Gene	Forward	Reverse
Gapdh (mouse)	TGCACCACCAACTGCTTAG	GGATGCAGGGATGATGTTC
Thy1.1 (mouse)	GCCGCCATGAGAATAACA	GCTAGGGTAAGGACCTTGAT
Perforin (mouse)	GAGAAGACCTATCAGGACCA	AGCCTGTGGTAAGCATG
Gzma (mouse)	TGATGTGAAACCAGGAACCA	ATGCCTCGCAAAATACCATC
Gzmb (mouse)	GACCCAGCAAGTCATCCCTA	CACACTCCCGATCCTTCTGT
Gzmk (mouse)	CCGTGGTTTTAGGAGCACAT	CAGGGTATCAGAGGCGGTTA
Tcf7 (mouse)	CAATCTGCTCATGCCCTACC	CTTGCTTCTGGCTGATGTCC

Tcf1, GZMA, GZMB, IL-2, IFN-γ, and TNF-α assays were performed using the Transcription Factor Buffer Set (BD Biosciences), Intracellular Fixation & Permeabilization Buffer Set (eBioscience), or Fixation/Permeabilization Solution Kit (BD Biosciences) according to each manufacturer's recommendations. Samples were analyzed using an LSRII or an LSRFortessa (BD Biosciences) with FlowJo software (Tree Star).

Cytokine release assay. The amount of IL-2, IFN-γ, and TNF-α in coculture supernatants was determined by using mouse IL-2–specific, TNF-α–specific, and IFN-γ–specific ELISA kits (BD Biosciences) according to the manufacturer's instructions. To obtain culture supernatants, each tumor cell line (1×10^4 cells/well) and effector T cells (3×10^4 or 1×10^5 cells/well) were cultured alone and together on 96-well plates (0.2 mL/well) for 24 hours. The resulting cell-cultured media supernatants were harvested and centrifuged to remove cellular debris.

In vitro restimulation of flow-sorted adoptively transferred Pmel-1 T cells. For in vitro restimulation of adoptively transferred Pmel-1 T cells, blood and splenocytes were harvested from ACT-treated, B16-bearing, female C57BL/6 mice 7 days after adoptive transfer of Pmel-1 T cells. Three subsets of Pmel-1 T cells defined by their CX3CR1 expression ($CX3CR1^{-}$, $CX3CR1^{int}$, and $CX3CR1^{hi}$) were flow-sorted with FACSAria sorter (BD Biosciences). For 4 days, 1×10^5 sorted cells were cocultured with 1 μM hgp100 peptide and 5×10^4 mitomycin-C–treated splenocytes from B6 mice.

RT and real-time PCR analysis. Total RNA samples were isolated with TRIzol reagent (Invitrogen, Thermo Fisher Scientific) and purified according to the manufacturer's instructions. Total RNA was used for cDNA synthesis by RT-PCR with ImProm-II Reverse Transcription System (Promega) with random primers according to the manufacturer's instructions. cDNA was amplified by Maxima SYBR Green/ROX qPCR Master Mix (Thermo Fisher Scientific), with the Bio-Rad CFX96 Real-Time Detection System (Bio-Rad) and the sets of primers shown in Table 2.

In vitro cytotoxicity assay. Luciferase-expressing target cells were seeded in triplicate in 96-well plates at 1×10^4 cells/well at various effector-to-target ratios. Effector and tumor cells were allowed to interact at 37°C for 24 hours. A final concentration of 0.15 mg/mL D-Luciferin (Gold Biotechnology) was added to each well. Luciferase bioluminescence was measured by the Xenogen In Vivo Imaging System 100 (PerkinElmer) and Living Image software (Caliper Life Sciences).

Patient tumor cell samples. Patients were eligible for this study if they were 18 years of age or older and were undergoing resection of metastasis and/or regional LN dissection for clinically evident regional or distant metastases of melanoma. Freshly resected tumors were sent from the surgery suite to the tissue procurement core in sterile containers. The tumor material not required for histopathologic diagnosis was placed in collecting medium, RPMI 1640 supplemented with 200 μg/mL gentamicin, 5 μg/mL ciprofloxacin, 20 μg/mL metronidazole, 100 U/mL penicillin, 50 μg/mL streptomycin, 25 μg/mL vancomycin, and 2.5 μg/mL fungizone (all from Life Technologies), as described before (54). Under sterile conditions, tumors were dissected away from adjacent normal tissue and stroma. Single-cell suspensions were obtained by mechanical dispersion consisting of two 30-minute incubations of 2.5 g minced melanoma tumor at 37°C, 5% CO_2, in 5 mL RPMI 1640 (Life Technologies) and Tumor Dissociation Kit (Miltenyi Biotec) in C Tubes (Miltenyi Biotec) interspersed with 3 mechanical dispersions on a GentleMACS dissociator (Miltenyi Biotec). The tumor cell suspensions were then filtered through a cell strainer (70 μm; BD Biosciences). TILs and tumor cells were isolated with a 2-step density-gradient centrifugation (54). Tumor suspension in RPMI was layered onto a 2-step gradient with a lower step of 100% Ficoll and a middle step of 75% Ficoll and 25% complete medium. After 20 minutes' centrifugation at 400 *g*, the interfaces were collected for flow cytometric analysis (54).

Statistics. Statistical analysis was performed using *t* test or Mann-Whitney *U* test for comparisons between 2 groups, 1-way repeated-measures ANOVA with Tukey-adjusted multiple comparisons for comparisons of more than 2 groups, or the Mantel-Cox method (log-rank test) for survival analysis using GraphPad Prism 7.03 (GraphPad Software). All tests were 2 sided and $P < 0.05$ was considered statistically significant. Data are presented as mean ± SEM.

Study approval. Human melanoma cell samples were obtained from the patients who signed the informed consent document under the protocol (HUM00054459) approved by the Institutional Review Board of the University of Michigan. All animal studies were reviewed and approved by the Roswell Park institutional animal care and use program and facilities (protocols 1316M and 1356M). All aspects of animal research and husbandry were conducted in accordance with the federal Animal Welfare Act and the NIH's *Guide for the Care and Use of Laboratory Animals* (National Academies Press, 2011).

Author contributions

TY contributed development of methodology, acquisition of data, analysis and interpretation of data, and writing, review, and revision of the manuscript. TH contributed development of methodology, acquisition of data, analysis and interpretation of data, and review and revision of the manuscript. TO contributed acquisition of data, analysis and interpretation of data, and review and revision of the manuscript. HS contributed acquisition of material and review and revision of the manuscript. KA contributed analysis and interpretation of data and review and revision of the manuscript. MSS contributed acquisition of material and review and revision of the manuscript. AEC contributed acquisition of material and review and revision of the manuscript. KO contributed acquisition of material and review of the manuscript. FI contributed conception and design, development of methodology, acquisition of data, analysis and interpretation of data, and writing, reviewing, and finalizing the manuscript.

Acknowledgments

We acknowledge Prometheus Laboratories Inc. for providing rhIL-2. This work was supported by Roswell Park Alliance Foundation and the National Cancer Institute (NCI) of the NIH Cancer Center Support Grant 5P30 CA016056 involving the use of Roswell Park's Flow and Image Cytometry. FI is a Young Investigator supported by the Melanoma Research Alliance and the NIH/NCI K08CA197966. TY is supported by Astellas Foundation for Research on Metabolic Disorders and The Nakatomi Foundation. TO is supported by Uehara Memorial Foundation. We thank Dr. AJ Robert McGray and Dr. Kitty de Jong for technical assistance and Dr. Suzanne M. Hess and Ms. Judith Epstein for administrative assistance.

Address correspondence to: Fumito Ito, Elm and Carlton Streets, Buffalo, New York 14263, USA. Phone: 716.845.1300; Email: fumito.ito@roswellpark.org.

1. Zhang N, Bevan MJ. CD8(+) T cells: foot soldiers of the immune system. *Immunity*. 2011;35(2):161–168.
2. Stemberger C, et al. A single naive CD8+ T cell precursor can develop into diverse effector and memory subsets. *Immunity*. 2007;27(6):985–997.
3. Williams MA, Bevan MJ. Effector and memory CTL differentiation. *Annu Rev Immunol*. 2007;25:171–192.
4. Fridman WH, Pagès F, Sautès-Fridman C, Galon J. The immune contexture in human tumours: impact on clinical outcome. *Nat Rev Cancer*. 2012;12(4):298–306.
5. Boon T, Coulie PG, Van den Eynde BJ, van der Bruggen P. Human T cell responses against melanoma. *Annu Rev Immunol*. 2006;24:175–208.
6. Rosenberg SA, et al. Tumor progression can occur despite the induction of very high levels of self/tumor antigen-specific CD8+ T cells in patients with melanoma. *J Immunol*. 2005;175(9):6169–6176.
7. Joyce JA, Fearon DT. T cell exclusion, immune privilege, and the tumor microenvironment. *Science*. 2015;348(6230):74–80.
8. Thommen DS, Schumacher TN. T Cell dysfunction in cancer. *Cancer Cell*. 2018;33(4):547–562.
9. Wherry EJ, Kurachi M. Molecular and cellular insights into T cell exhaustion. *Nat Rev Immunol*. 2015;15(8):486–499.
10. Topalian SL, et al. Safety, activity, and immune correlates of anti–PD-1 antibody in cancer. *N Engl J Med*. 2012;366(26):2443–2454.
11. Hodi FS, et al. Improved survival with ipilimumab in patients with metastatic melanoma. *N Engl J Med*. 2010;363(8):711–723.
12. Gattinoni L, et al. Acquisition of full effector function in vitro paradoxically impairs the in vivo antitumor efficacy of adoptively transferred CD8+ T cells. *J Clin Invest*. 2005;115(6):1616–1626.
13. Restifo NP, Dudley ME, Rosenberg SA. Adoptive immunotherapy for cancer: harnessing the T cell response. *Nat Rev Immunol*. 2012;12(4):269–281.
14. He R, et al. Follicular CXCR5- expressing CD8(+) T cells curtail chronic viral infection. *Nature*. 2016;537(7620):412–428.
15. Im SJ, et al. Defining CD8+ T cells that provide the proliferative burst after PD-1 therapy. *Nature*. 2016;537(7620):417–421.

16. Gerlach C, et al. The chemokine receptor CX3CR1 defines 3 antigen-experienced CD8 T cell subsets with distinct roles in immune surveillance and homeostasis. *Immunity*. 2016;45(6):1270–1284.
17. Overwijk WW, et al. gp100/pmel 17 is a murine tumor rejection antigen: induction of "self"-reactive, tumoricidal T cells using high-affinity, altered peptide ligand. *J Exp Med*. 1998;188(2):277–286.
18. Saito H, Okita K, Chang AE, Ito F. Adoptive transfer of CD8+ T cells generated from induced pluripotent stem cells triggers regressions of large tumors along with immunological memory. *Cancer Res*. 2016;76(12):3473–3483.
19. Hailemichael Y, et al. Persistent antigen at vaccination sites induces tumor-specific CD8+ T cell sequestration, dysfunction and deletion. *Nat Med*. 2013;19(4):465–472.
20. Kaech SM, Tan JT, Wherry EJ, Konieczny BT, Surh CD, Ahmed R. Selective expression of the interleukin 7 receptor identifies effector CD8 T cells that give rise to long-lived memory cells. *Nat Immunol*. 2003;4(12):1191–1198.
21. Gattinoni L, Klebanoff CA, Restifo NP. Paths to stemness: building the ultimate antitumour T cell. *Nat Rev Cancer*. 2012;12(10):671–684.
22. Germar K, et al. T-cell factor 1 is a gatekeeper for T-cell specification in response to Notch signaling. *Proc Natl Acad Sci U S A*. 2011;108(50):20060–20065.
23. Weber BN, et al. A critical role for TCF-1 in T-lineage specification and differentiation. *Nature*. 2011;476(7358):63–68.
24. Jeannet G, Boudousquié C, Gardiol N, Kang J, Huelsken J, Held W. Essential role of the Wnt pathway effector Tcf-1 for the establishment of functional CD8 T cell memory. *Proc Natl Acad Sci U S A*. 2010;107(21):9777–9782.
25. Zhou X, Yu S, Zhao DM, Harty JT, Badovinac VP, Xue HH. Differentiation and persistence of memory CD8(+) T cells depend on T cell factor 1. *Immunity*. 2010;33(2):229–240.
26. Utzschneider DT, et al. T cell factor 1-expressing memory-like CD8(+) T Cells sustain the immune response to chronic viral infections. *Immunity*. 2016;45(2):415–427.
27. Wu T, et al. The TCF1-Bcl6 axis counteracts type I interferon to repress exhaustion and maintain T cell stemness. *Sci Immunol*. 2016;1(6):eaai8593.
28. Miller BC, et al. Subsets of exhausted $CD8^+$ T cells differentially mediate tumor control and respond to checkpoint blockade. *Nat Immunol*. 2019;20(3):326–336.
29. Siddiqui I, et al. Intratumoral $Tcf1^+PD\text{-}1^+CD8^+$ T cells with stem-like properties promote tumor control in response to vaccination and checkpoint blockade immunotherapy. *Immunity*. 2019;50(1):195–211.e10.
30. Chen Z, et al. TCF-1-centered transcriptional network drives an effector versus exhausted CD8 T cell-fate decision. *Immunity*. 2019;51(5):840–855.e5.
31. Hudson WH, et al. Proliferating transitory T cells with an effector-like transcriptional signature emerge from $PD\text{-}1^+$ stem-like $CD8^+$ T cells during chronic infection. *Immunity*. 2019;51(6):1043–1058.e4.
32. Yu YR, Fong AM, Combadiere C, Gao JL, Murphy PM, Patel DD. Defective antitumor responses in CX3CR1-deficient mice. *Int J Cancer*. 2007;121(2):316–322.
33. Yan Y, et al. CX3CR1 identifies PD-1 therapy-responsive CD8+ T cells that withstand chemotherapy during cancer chemoimmunotherapy. *JCI Insight*. 2018;3(8):97828.
34. Xin H, et al. Antitumor immune response by CX3CL1 fractalkine gene transfer depends on both NK and T cells. *Eur J Immunol*. 2005;35(5):1371–1380.
35. Zeng Y, et al. Fractalkine (CX3CL1)- and interleukin-2-enriched neuroblastoma microenvironment induces eradication of metastases mediated by T cells and natural killer cells. *Cancer Res*. 2007;67(5):2331–2338.
36. Zander R, et al. $CD4^+$ T cell help is required for the formation of a cytolytic $CD8^+$ T cell subset that protects against chronic infection and cancer. *Immunity*. 2019;51(6):1028–1042.e4.
37. Nishimura M, et al. Dual functions of fractalkine/CX3C ligand 1 in trafficking of perforin+/granzyme B+ cytotoxic effector lymphocytes that are defined by CX3CR1 expression. *J Immunol*. 2002;168(12):6173–6180.
38. Diehl GE, et al. Microbiota restricts trafficking of bacteria to mesenteric lymph nodes by CX(3)CR1(hi) cells. *Nature*. 2013;494(7435):116–120.
39. Vacchio MS, et al. A ThPOK-LRF transcriptional node maintains the integrity and effector potential of post-thymic CD4+ T cells. *Nat Immunol*. 2014;15(10):947–956.
40. Blackburn SD, Shin H, Freeman GJ, Wherry EJ. Selective expansion of a subset of exhausted CD8 T cells by alphaPD-L1 blockade. *Proc Natl Acad Sci U S A*. 2008;105(39):15016–15021.
41. Böttcher JP, et al. Functional classification of memory CD8(+) T cells by CX3CR1 expression. *Nat Commun*. 2015;6:8306.
42. Gordon CL, et al. Induction and maintenance of CX3CR1-intermediate peripheral memory $CD8^+$ T cells by persistent viruses and vaccines. *Cell Rep*. 2018;23(3):768–782.
43. Ahrends T, et al. CD4(+) T cell help confers a cytotoxic t cell effector program including coinhibitory receptor downregulation and increased tissue invasiveness. *Immunity*. 2017;47(5):848–861.e5.
44. Guo J, et al. Fractalkine transgene induces T-cell-dependent antitumor immunity through chemoattraction and activation of dendritic cells. *Int J Cancer*. 2003;103(2):212–20.
45. Kee JY, et al. Antitumor immune activity by chemokine CX3CL1 in an orthotopic implantation of lung cancer model in vivo. *Mol Clin Oncol*. 2013;1(1):35–40.
46. Wallin JJ, et al. Atezolizumab in combination with bevacizumab enhances antigen-specific T-cell migration in metastatic renal cell carcinoma. *Nat Commun*. 2016;7:12624.
47. Joshi NS, et al. Inflammation directs memory precursor and short-lived effector CD8(+) T cell fates via the graded expression of T-bet transcription factor. *Immunity*. 2007;27(2):281–295.
48. Precopio ML, et al. Immunization with vaccinia virus induces polyfunctional and phenotypically distinctive CD8(+) T cell responses. *J Exp Med*. 2007;204(6):1405–1416.
49. Saparov A, et al. Interleukin-2 expression by a subpopulation of primary T cells is linked to enhanced memory/effector function. *Immunity*. 1999;11(3):271–280.
50. Angelosanto JM, Blackburn SD, Crawford A, Wherry EJ. Progressive loss of memory T cell potential and commitment to exhaustion during chronic viral infection. *J Virol*. 2012;86(15):8161–8170.

51. Schietinger A, Greenberg PD. Tolerance and exhaustion: defining mechanisms of T cell dysfunction. *Trends Immunol*. 2014;35(2):51–60.
52. Campeau E, et al. A versatile viral system for expression and depletion of proteins in mammalian cells. *PLoS One*. 2009;4(8):e6529.
53. Rosenberg SA, et al. Durable complete responses in heavily pretreated patients with metastatic melanoma using T-cell transfer immunotherapy. *Clin Cancer Res*. 2011;17(13):4550–4557.
54. Saito H, Okita K, Fusaki N, Sabel MS, Chang AE, Ito F. Reprogramming of melanoma tumor-infiltrating lymphocytes to induced pluripotent stem cells. *Stem Cells Int*. 2016;2016(8394960):11.